AIAA/AAS Astrodynamics Specialist Conference and Exhibit
16 - 19 August 2004, Providence, Rhode Island

AIAA 2004-5213

Differential Orbit Element Constraints for Coulomb Satellite Formations

Hanspeter Schaub* and Mischa Kim †
Virginia Polytechnic Institute, Blacksburg, VA 24091-0203

Recently the concept of controlling the relative motion of spacecraft using electrostatic charging has been proposed. For tight spacecraft formations with separation distances ranging from 10–100 meters, the Coulomb forces between the spacecraft can be exploited to provide a very fuel and power efficient means of propulsion. As the charge of a single craft is varied, the relative motion of the entire formation is affected. The Coulomb force vector a craft experiences is restricted to be directed along the relative position vector, which results in constraints being imposed on how the Coulomb force can be used to control a formation. This paper investigates how the conservation of angular momentum and the formation center of mass limits the types of relative orbits that can be controlled. Considering the spacecraft formation to be a system of N particles, this internal force can not change the inertial system angular momentum vector. The center of mass definition and angular momentum constraint are expressed using differential orbit elements to describe the relative motion. First order transformations to the nonlinear solutions are presented. Their accuracy is evaluated both analytically and using numerical simulations.

I. Introduction

SPACECRAFT formation flying control is a challenging research thrust requiring a fundamental understanding of both orbital mechanics and control theory. Typically, the amount of propellant aboard a craft is limited. Nevertheless, even with a carefully chosen relative orbit geometry, the control system typically needs to perform minor orbit corrections periodically to maintain the formation. Typical spacecraft interferometry missions consider separation distances ranging from hundreds of meters to multiple kilometers. Large baselines are used to provide highly accurate sensing of a narrow field of view. The forces required for a continuous thrust propulsion system to maintain a relative orbit are of the order of milli-Newtons or less. Pulsed-Plasma Thrusters (PPTs) and other ion engines are considered as the primary relative navigation propulsion method. The thrust is achieved by expelling charged ions at a very high velocity. To achieve high escape velocities, relatively large amounts of electrical power must be provided. Because the exhaust plume contains toxic chemicals that could damage another spacecraft or its sensors, care must be taken that the ion engine exhaust does not hit another craft. For formations with relative separations in the order of kilometers, the exhaust issue is not of concern.

Consider a tight formation to be defined as having spacecraft separation distances ranging between 10 and 100 meters. Such clusters could be used to perform high accuracy, very wide field of view missions at Geostationary Orbits (GEO). For example, 20-30 meter formations at GEO could observe the entire hemisphere with a meter level resolution with infinite dwell time. Alternatively, tight formations could be used to measure local gradients of magnetic or gravitational fields. Yet another application exploits the Coulomb forces to navigate a sensor about a larger spacecraft. In all of these scenarios, the ion engine exhaust plume issues is one of the primary mission concerns. However, with all craft flying in close proximity, collision avoidance and – in particular – fuel expenditure to perform the greatly increased number of relative orbit corrections are of major concern. In Reference 1 the use of electrostatic charging is used as a means to perform relative orbit control. It was found that milli-Newton levels of thrust could

*Assistant Professor, Aerospace and Ocean Engineering Department, Virginia Tech, Blacksburg. AIAA Senior Member
†Graduate Student, Aerospace and Ocean Engineering Department, Virginia Tech, Blacksburg. AIAA Student Member

be achieved between the vehicles with typical power requirements of < 1 Watt. Calculated I_{sp} fuel efficiencies were as high as 10^{10}–10^{13} seconds, rendering this mode of propulsion essentially propellantless. Measured spacecraft charging data obtained by the SCATHA GEO mission in 1979 verified that a craft can charge to high voltages in low space plasma environments such as GEO.[2] More recently, the CLUSTERS mission demonstrated the feasibility to control the spacecraft charge and maintain a near-zero voltage level.[3] Note that Coulomb force control is only effective for relatively tight formation/proximity flying scenarios of 10–100 meters due to the $1/r^2$ behavior of the Coulomb electrostatic force magnitude, r being the spacecraft separation distance. For minimum separation distances larger than that, the required spacecraft charging levels simply become impractical due to differential charging issues. Additionally, Coulomb force effectiveness is diminished in a space plasma environment. The reduced effectiveness is measured through the Debye length, which indicates the exponential decay e^{-r/λ_d} of the electrostatic field strength.[4,5] Because λ_d is in the order of centimeter for Low Earth Orbits (LEO), the Coulomb satellite concept is not practical at low altitudes. However, at GEO it was found that λ_d values are in the order of 100–1000 meters, making Coulomb formation flying (CFF) feasible at higher altitudes.

References 1 and 6 discuss interesting steady-state solutions that exist for the charged relative orbit equations of motion equations. The authors show how such charged formations are able to establish fixed relative positions as seen by the rotating Hill coordinate frame. As a result the individual spacecraft can be shown to perform non-Keplerian orbits to maintain their formation position. Both in-plane and general three-dimensional steady-state equilibrium conditions were found. However, none of these formation shapes were found to be controllable. Nonlinear charging control laws were investigated for a two-satellite formation in Reference 7, and for a larger cluster of Coulomb satellites in Reference 8. An orbit element difference approach was used to describe and control the relative motion. However, in these control developments, only general stability properties were provided. Asymptotic convergence was only discussed for algorithms controlling semi-major axis exclusively. For example, it is intuitive that the inter-spacecraft Coulomb forces cannot be used to change a relative orbit from being an in-plane formation to having out-of-plane components.

Since Coulomb force control inherently only allows for relative motion control (spacecraft are pushing and pulling off each other), it is natural to describe relative motion of a Coulomb formation with respect to the formation center of mass (CM). The single-craft control strategies in References 7 and 8 identify the formation chief position as the formation center of mass. Furthermore, these papers assume the Coulomb formation chief to be moving in a Keplerian, unperturbed orbit. As shown in Reference 9, these assumptions are valid approximations and particularly feasible for small formations using Coulomb thrusting. Reference 9 examines relative motion constraints of Coulomb formations for satellite motion described using either inertial or formation-center-of-mass relative position vectors.

This paper investigates how conservation of inertial angular momentum and the formation center of mass (barycenter) definition constrain the evolution of Coulomb formations if the relative motion is expressed using differential orbit elements. The formation center of mass definition is a simple linear relationship only when using Cartesian coordinates. On the other hand, the barycenter definition becomes a nonlinear function using an orbit elements system description. Similarly, the precise momentum constraint using orbit element differences is a complex function. First order approximations are introduced for these transformations and their accuracy is discussed both analytically and through numerical illustrations. In particular, the concept of an orbit element based formation barycenter is introduced and compared to the classical Cartesian formation barycenter. When controlling Coulomb formations, it is more meaningful to describe the formation with respect to the orbit element barycenter versus the Cartesian formation barycenter. The presented first order orbit element constraints on Coulomb formations can be used in control analysis research to investigate convergence and feasible relative motion.

II. Problem Statement

Rather than using traditional Cartesian coordinates with respect to the rotating Hill frame, classical orbit elements $\boldsymbol{oe} = (a, e, i, \Omega, \omega, M_0)$ are used to describe the satellite motion. Note that semi-major axis a, eccentricity e, orbit inclination angle i, ascending node angle Ω and argument of periapses ω, as well as initial mean anomaly M_0, are constants of the unperturbed orbital motion (Keplerian motion case). To describe the satellite relative motion, differences in orbit elements $\delta\boldsymbol{oe}$ are used. For unperturbed, uncontrolled relative motion, these differenced elements are constants, as well.

It is convenient to describe Coulomb formations relative to the formation center-of-mass or barycenter $\boldsymbol{R}_c$. Since the electrostatic Coulomb force is a formation-internal force, the control can not change the formation inertial angular momentum. If $\boldsymbol{h}_i$ is the angular momentum per unit mass of the i^{th} satellite, then the formation inertial angular

momentum

$$\boldsymbol{h} = \sum_{i=1}^{N} \boldsymbol{h}_i \tag{1}$$

must be a constant of motion. This conservation law imposes three constraints onto the charged relative motion dynamics. As pointed out before, the conservation of angular momentum is readily expressed using either inertial Cartesian position and velocity vectors $(\boldsymbol{R}_i, \dot{\boldsymbol{R}}_i)$ or inertial orbit elements $\boldsymbol{oe}$. However, the momentum constraint, as well as the formation barycenter definition, are more complex if relative position coordinates $\delta\boldsymbol{oe}$ are employed. Of interest are analytic approximations of the momentum and barycenter expressions using orbit element differences. While momentum conservation is specific to the study of Coulomb formations, the barycenter discussion is applicable to general spacecraft formations.

III. Center of Mass Definition

Let us first investigate the formation barycenter definition using differenced orbit elements. The inertial position and velocity vectors of the formation center of mass are traditionally defined using inertial Cartesian position and velocity vectors as

$$\boldsymbol{R}_c = \frac{1}{M} \sum_{i=1}^{N} m_i \boldsymbol{R}_i \tag{2}$$

$$\dot{\boldsymbol{R}}_c = \frac{1}{M} \sum_{i=1}^{N} m_i \dot{\boldsymbol{R}}_i \tag{3}$$

where $M = \sum_{i=1}^{N} m_i$ is the total formation mass. Eq. (2) defines the true formation center of mass position vector. Later on, approximate solutions are compared to the classical formulation (2). Using relative position coordinates $\boldsymbol{r}_i = \boldsymbol{R}_i - \boldsymbol{R}_c$ with respect to the formation barycenter, Eq. (2) can be rewritten as

$$\sum_{i=1}^{N} m_i \, \boldsymbol{r}_i = \boldsymbol{0} \tag{4}$$

Note that Eq. (4) is a vector equation and must hold for any coordinate frame choice to express the vector components. Let $\boldsymbol{r}_i$ vector components be expressed in the chief Local-Vertical-Local-Horizontal (LVLH) or Hill frame $\mathcal{H}$ as[10]

$${}^{\mathcal{H}}\boldsymbol{r}_i = \begin{pmatrix} x_i \\ y_i \\ z_i \end{pmatrix} \tag{5}$$

Next, let the non-dimensional relative position coordinates be defined through

$$u_i = \frac{x_i}{R_c} \qquad v_i = \frac{y_i}{R_c} \qquad w_i = \frac{z_i}{R_c} \tag{6}$$

Note that the formation barycenter radius R_c is time varying in general (elliptic orbits). An equivalent expression for the center of mass condition in Eq. (4) is expressed using (u, v, w) as

$$\sum_{i=1}^{N} m_i u_i = \sum_{i=1}^{N} m_i v_i = \sum_{i=1}^{N} m_i w_i = 0 \tag{7}$$

If the relative motion is expressed using Cartesian coordinates, as is commonly done when using the Clohessy-Wiltshire-Hill equations,[10–12] center of mass definitions in either Eq. (2) or (7) could be used directly. However, if the relative motion is expressed using orbit element differences, the center of mass conditions are not obvious, especially if the chief orbit is allowed to be highly eccentric.

For the subsequent analysis the following notational short hand is used: orbit elements without subscripts are implied to denote the formation chief or center of mass. To find approximate first order center of mass conditions

using orbit element differences, we can exploit a relative motion description presented in References 13 and 14. Using classical orbit element differences, non-dimensional (u, v, w) motion equations of each satellite can be written as

$$u_i = \frac{\delta a_i}{a} - \frac{e\,\delta e_i}{2\eta^2} + \frac{1}{\eta^2}\delta_{u_i}\cos\left(f - f_{u_i}\right) + \frac{e}{2\eta^2}\delta_{u_i}\cos\left(2f - f_{u_i}\right) + \mathcal{O}(\delta\alpha e^2) \tag{8}$$

$$\begin{aligned} v_i = {} & \left(\left(1 + \frac{e^2}{2}\right)\frac{\delta M_i}{\eta^2} + \delta\omega_i + \cos i\,\delta\Omega_i\right) - 2\frac{\delta_{u_i}}{\eta^2}\sin\left(f - f_{u_i}\right) \\ & - \frac{\delta_{u_i}}{\eta^2}\frac{e}{2}\sin\left(2f - f_{u_i}\right) + \mathcal{O}(\delta\alpha e^2) \end{aligned} \tag{9}$$

$$w_i = \sqrt{\delta i_i^2 + \sin^2 i\,\delta\Omega_i^2}\cos\left(\theta - \theta_{w_i}\right) + \mathcal{O}(\delta\alpha e^2) \tag{10}$$

where

$$\delta_{u_i} = \sqrt{\frac{e^2\,\delta M_i^2}{\eta^2} + \delta e_i^2} \tag{11}$$

$$f_{u_i} = \arctan\left(\frac{e\,\delta M_i}{-\eta\delta e_i}\right) \tag{12}$$

$$\theta_{w_i} = \arctan\left(\frac{\delta i_i}{-\sin i\,\delta\Omega}\right) \tag{13}$$

This relative motion description is convenient because it provides a direct description of the general relative motion in terms of secular offsets and repeating trigonometric terms. Contrary to the analytical solution of the Clohessy-Wiltshire-Hill equations, the first order relative motion solution is valid for both circular and elliptic chief motions.

For the barycenter conditions in Eq. (7) to be satisfied, the sum of the constant terms, terms depending on $\cos(f - f_{u_i})$, terms depending on $\cos(2f - f_{u_i})$, terms depending on $\sin(f - f_{u_i})$, and terms depending on $\sin(2f - f_{u_i})$ must vanish independently. Let us first analyze the $\sum_{i=1}^{N} m_i u_i = 0$ condition. For the constant terms to vanish, it must be true that

$$\sum_{i=1}^{N} m_i\left(\frac{\delta a_i}{a} - \frac{e\,\delta e_i}{2\eta^2}\right) = 0 \tag{14}$$

For the terms depending on $\cos(f - f_{u_i})$ to vanish, we notice that

$$\sum_{i=1}^{N}\frac{m_i}{\eta^2}\delta_{u_i}\cos(f - f_{u_i}) = \sum_{i=1}^{N}\frac{m_i}{\eta^2}\sqrt{\frac{e^2\,\delta M_i^2}{\eta^2} + \delta e_i^2}\cos(f - f_{u_i}) = 0 \tag{15}$$

must hold. Note that the different phase angles f_{u_i} make it non-trivial to further refine this condition. Using the trigonometric identity

$$A\sin f + B\cos f = \sqrt{A^2 + B^2}\cos\left[f - \tan^{-1}\left(\frac{A}{B}\right)\right] \tag{16}$$

we can rewrite condition (15) as

$$\begin{aligned} 0 &= \sum_{i=1}^{N}\frac{m_i}{\eta^2}\left(\frac{e\,\delta M_i}{\eta}\sin f - \delta e_i\cos f\right) \\ &= \frac{1}{\eta^2}\left[\left(\sum_{i=1}^{N}\frac{m_i\,e\,\delta M_i}{\eta}\right)\sin f + \left(\sum_{i=1}^{N}(-m_i\,\delta e_i)\right)\cos f\right] \\ &= \frac{1}{\eta^2}\sqrt{\left(\sum_{i=1}^{N}\frac{m_i\,e\,\delta M_i}{\eta}\right)^2 + \left(\sum_{i=1}^{N}(-m_i\,\delta e_i)\right)^2}\cos\left(f - \hat{f}_u\right) \end{aligned} \tag{17}$$

where

$$\hat{f}_u = \tan^{-1}\left(\frac{\sum_{i=1}^{N} \frac{m_i e \delta M_i}{\eta}}{\sum_{i=1}^{N}(-m_i\,\delta e_i)}\right) \tag{18}$$

With the last transformation, an expression is obtained where the phase angle is constant for all summation terms. Hence, for Eq. (17) to be satisfied for all time, we find that

$$\sum_{i=1}^{N} m_i\,\delta e_i = 0 \tag{19}$$

$$\sum_{i=1}^{N} m_i\,\delta M_i = 0 \tag{20}$$

must be true. Revisiting the condition in Eq. (14), Eq. (19) implies that

$$\sum_{i=1}^{N} m_i\,\delta a_i = 0 \tag{21}$$

No new conditions on the orbit element differences are found examining the $\cos(2f - f_{u_i})$ terms of $\sum_{i=1}^{N} m_i u_i = 0$.

Next, let us examine the condition $\sum_{i=1}^{N} m_i v_i = 0$. The terms containing $\sin(f - f_{u_i})$ and $\sin(2f - f_{u_i})$ do not provide any new information. Equivalent transformations can be performed to yield conditions in Eqs. (19) and (20). Thus, let us focus on the constant terms of v_i and examine under what conditions their weighted sum vanishes.

$$\sum_{i=1}^{N} m_i \left[\left(1 + \frac{e^2}{2}\right)\frac{\delta M_i}{\eta^2} + \delta\omega_i + \cos i\,\delta\Omega_i\right] = 0 \tag{22}$$

which simplifies (using Eq. (20)) to

$$\sum_{i=1}^{N} m_i\,(\delta\omega_i + \cos i\,\delta\Omega_i) = 0 \tag{23}$$

This expression will be refined later on in the development. The final condition $\sum_{i=1}^{N} m_i w_i = 0$ of Eq. (7), yields

$$\sum_{i=1}^{N} m_i \sqrt{\delta i_i^2 + \sin^2 i\,\delta\Omega_i^2}\cos\left(\theta - \theta_{w_i}\right) = 0 \tag{24}$$

Using similar trigonometric transformations as were used examining the first moment constraint $\sum_{i=1}^{N} m_i u_i = 0$, the following condition is found:

$$\sqrt{\left(\sum_{i=1}^{N} m_i\,\delta i_i\right)^2 + \sin^2 i\left(\sum_{i=1}^{N} m_i\,\delta\Omega_i\right)^2}\cos(\theta - \hat{\theta}_w) = 0 \tag{25}$$

which leads to the following orbit element constraints:

$$\sum_{i=1}^{N} m_i\,\delta i_i = 0 \tag{26}$$

$$\sum_{i=1}^{N} m_i\,\delta\Omega_i = 0 \tag{27}$$

Substituting Eq. (27) into the condition in Eq. (23) we obtain

$$\sum_{i=1}^{N} m_i\,\delta\omega_i = 0 \tag{28}$$

At first glance it might be odd that three Cartesian coordinate constraint equations in Eq. (7) yield six orbit element difference constraints. Note however, that the full nonlinear mapping between orbit elements and Cartesian coordinates also involves Cartesian velocities. Therefore, orbit elements are really a blended measure of both position and velocity information, that is, Eq. (7) directly implies

$$\sum_{i=1}^{N} m_i \dot{u}_i = \sum_{i=1}^{N} m_i \dot{v}_i = \sum_{i=1}^{N} m_i \dot{w}_i = 0 \tag{29}$$

Given relative position vectors of $(N-1)$ satellites with respect to the center of mass, Eq. (7) uniquely determines the N^{th} satellite relative position vector. Similarly, Eq. (29) determines the N^{th} satellite relative velocity vector given $(N-1)$ satellite relative velocity vectors. The equivalent orbit element difference expressions are summarized as

$$\sum_{i=1}^{N} m_i \, \delta a_i = 0 \qquad \sum_{i=1}^{N} m_i \, \delta e_i = 0 \qquad \sum_{i=1}^{N} m_i \, \delta i_i = 0 \tag{30a}$$

$$\sum_{i=1}^{N} m_i \, \delta \Omega_i = 0 \qquad \sum_{i=1}^{N} m_i \, \delta \omega_i = 0 \qquad \sum_{i=1}^{N} m_i \, \delta M_i = 0 \tag{30b}$$

Note that Eqs. (30) are only first order approximations of the formation center of mass definition. While both the Cartesian coordinate center of mass definition in Eq. (2) and (4) are rigorously true, the above orbit element difference conditions are first order approximations where we assume that the orbit element differences are small compared to the chief orbit elements. The result, that the mass-averaged sum of all relative orbit element differences must equal zero is equivalent to the Cartesian version in Eq. (4). For the sake of clarity, we refer to the mass-averaged orbit element difference location as the Orbit Element Barycenter (OEB). While not equal to the true Cartesian barycenter (CB) of the formation, the OEB is of value when describing and controlling formations. Consider a simple leader-follower 2-satellite formation in circular orbit. The true Cartesian barycenter rotates at the same orbit period as the satellites while having a slightly smaller orbit radius. Thus, the CB does not perform a Keplerian orbit motion.[9] Computing inertial formation barycenter position and velocity vectors $(\boldsymbol{R}_c, \dot{\boldsymbol{R}}_c)$, and translating these coordinates into equivalent orbit elements, we find that Keplerian motion predicts the CB to move faster than the satellites. Considering a control law that defines tracking errors with respect to the true formation Cartesian barycenter, the satellites are controlled with respect to a chief location which has a slightly different orbit period. In contrast, if the OEB is computed using Eq. (30) for the leader-follower example, the OEB assumes the same semi-major axis as the other two satellites. Both satellites and barycenter orbit at the same rate assuming Keplerian motion. Thus, the OEB does indeed evolve in a Keplerian manner. Note that the differences between the Cartesian and orbit element barycenter locations are very small. A detailed error analysis follows in a later section.

Constraints in Eq. (30) on the motion of Coulomb formations are useful when analyzing orbit element based feedback control laws. For example, for the dual-craft formation discussed in Reference 7, if $\delta a_1 \to 0$, the center of mass definition in Eq. (30) immediately implies that $\delta a_2 \to 0$, as well. In other words, for the 2-satellite system, showing convergence of one satellite is equivalent to showing convergence of the entire system.

IV. Angular Momentum

As pointed out before, the inertial angular momentum vector $\boldsymbol{H}$ is a constant of motion for the formation because Coulomb forces are internal forces of the spacecraft formation.[9] Let $\boldsymbol{R}_i$ be the i^{th} inertial spacecraft position vector and m_i be the associated constant spacecraft mass. The spacecraft cluster is assumed to contain N craft. The total formation angular momentum is then expressed as[10]

$$\boldsymbol{H} = \sum_{i=1}^{N} \boldsymbol{H}_i = \sum_{i=1}^{N} \boldsymbol{R}_i \times m_i \dot{\boldsymbol{R}}_i \tag{31}$$

The derivative taken here is an inertial time derivative. In astrodynamics, the massless momentum vector $\boldsymbol{h}$ is used to describe the momentum of a spacecraft.

$$\boldsymbol{h} = \boldsymbol{R} \times \dot{\boldsymbol{R}} = h \hat{\boldsymbol{i}}_h \tag{32}$$

The scalar h is the massless momentum magnitude of the spacecraft, while the unit vector $\hat{\boldsymbol{\imath}}_h$ is both a normal vector to the orbit plane and collinear with $\boldsymbol{h}$. Using the $\boldsymbol{h}$ definition, the formation angular momentum vector $\boldsymbol{H}$ can be written as

$$\boldsymbol{H} = \sum_{i=1}^{N} m_i(\boldsymbol{R}_i \times \dot{\boldsymbol{R}}_i) = \sum_{i=1}^{N} m_i \boldsymbol{h}_i \tag{33}$$

Note that h_i can be expressed in terms of the semi-major axis a and the eccentricity measure $\eta = \sqrt{1-e^2}$ as

$$h_i = \sqrt{\mu a_i}\eta_i \tag{34}$$

The orbit normal vector is obtained as[10]

$$\hat{\boldsymbol{\imath}}_{h_i} = \begin{pmatrix} \sin i_i \sin \Omega_i \\ -\sin i_i \cos \Omega_i \\ \cos i_i \end{pmatrix} \tag{35}$$

where the vector components are taken with respect to an inertial frame $\mathcal{N}$. Using Eqs. (34) and (35), the total inertial Coulomb formation angular momentum vector can be written as

$$\boldsymbol{H} = \sum_{i=1}^{N} m_i \sqrt{\mu a_i}\eta \begin{pmatrix} \sin i_i \sin \Omega_i \\ -\sin i_i \cos \Omega_i \\ \cos i_i \end{pmatrix} \tag{36}$$

If inertial orbit elements are used instead of orbit element differences to describe the satellite motion, then Eq. (36) provides the full nonlinear formation angular momentum relationship. Because $\boldsymbol{H}$ is constant, Eq. (36) provides three momentum constraints on the Coulomb relative motion. Note that so far no approximations have been introduced to the momentum constraints.

Using the formation Cartesian barycenter location $(\boldsymbol{R}_c, \dot{\boldsymbol{R}}_c)$, the inertial angular momentum of the formation center of mass is

$$\boldsymbol{H}_c = \boldsymbol{R}_c \times M\dot{\boldsymbol{R}}_c \tag{37}$$

Note that in general the total formation inertial angular momentum vector $\boldsymbol{H}$ is not equal to the formation chief angular momentum $\boldsymbol{H}_c$. However, if relative spacecraft distances are small compared to the inertial chief orbit radius, then $\boldsymbol{H}_c$ is reasonably close to the constant total formation inertial angular momentum, that is, $\boldsymbol{H}_c \approx \boldsymbol{H}$. Since the relative motion is expressed using orbit element differences, it is desirable to express the law of momentum conservation $\boldsymbol{H}(t) = \boldsymbol{H}(t_0)$ in terms of orbit element differences, as well. Note that Eq. (36) provides the complete nonlinear solution to the momentum conservation constraint. However, this vector equation is expressed in terms of orbit elements, and not orbit element differences. To rewrite the formation angular momentum in terms of orbit element differences, we expand $\boldsymbol{H}$ into a Taylor series about the center of mass states:

$$\begin{aligned} \boldsymbol{H} &= \boldsymbol{H}_c + \sum_{i=1}^{N} \left.\frac{\partial \boldsymbol{H}_i}{\partial \boldsymbol{\alpha e}_i}\right|_c \delta\boldsymbol{\alpha e}_i + \mathcal{O}\big(\delta\alpha_i^2\big) \\ &= \boldsymbol{H}_c + \sum_{i=1}^{N} \left.\frac{\partial \boldsymbol{h}_i}{\partial \boldsymbol{\alpha e}_i}\right|_c m_i\, \delta\boldsymbol{\alpha e}_i + \mathcal{O}\big(\delta\alpha_i^2\big) \\ &= \boldsymbol{H}_c + \left(\left.\frac{\partial \boldsymbol{h}}{\partial \boldsymbol{\alpha e}}\right|_c\right) \sum_{i=1}^{N} m_i\, \delta\boldsymbol{\alpha e}_i + \mathcal{O}\big(\delta\alpha_i^2\big) \\ &= \boldsymbol{H}_c + \mathcal{O}\big(\delta\alpha_i^2\big) \end{aligned} \tag{38}$$

In Eq. (38) corresponding first-order derivatives of the massless momentum vectors $\boldsymbol{h}_i$ are evaluated at the common formation center of mass and are therefore equal for all spacecraft. Pulling the derivatives in front of the summation sign and using Eqs. (30) we find the angular momentum of the formation barycenter to be a second order accurate approximation of the constant formation momentum vector $\boldsymbol{H}$. The next question is, what are the three momentum

constraint equations in terms of $\delta\boldsymbol{\alpha e}_i$? We point out that Eq. (38) do not yield any linear $\delta\boldsymbol{\alpha e}$ terms. The answer is that the three momentum constraint in terms of $\delta\boldsymbol{\alpha e}_i$ are inherently satisfied if the formation barycenter condition $\sum_{i=1}^{N} m_i \delta\boldsymbol{\alpha e}_i = 0$ is satisfied. Thus, to first order, the six conditions in Eq. (30) include both the three barycenter and three momentum constraints. Expressing the relative motion using the orbit element differences $\delta\boldsymbol{\alpha e}_i$, we must assure that

$$\sum_{i=1}^{N} m_i \delta\boldsymbol{\alpha e}_i = 0 \tag{39}$$

is true to satisfy all six combined barycenter and momentum CFF constraints of the barycenter-relative formation description using orbit element differences. In case the true nonlinear constraints are to be used instead of the first-order approximation, then the barycenter constraint in Eq. (4) and inertial momentum constraint in Eq. (36) must be satisfied. The first-order approximation provides a much more convenient form for analysis of feasible relative motion dynamics or charged relative motion control.

V. Center of Mass Definitions Error Analysis

As pointed out in a previous section, it proves advantageous for control analysis to define the center of mass of CFF using orbital elements and orbital element differences. Note, that conditions (30) specify the Cartesian formation barycenter location to first order, only. A more general nonlinear analysis shows how center of mass approximations in the orbital element space map into actual position and velocity errors in inertial space.

Let $\boldsymbol{\Gamma} : \mathbb{R}^6 \to \mathbb{R}^6$ be the nonlinear mapping that transforms orbital elements into cartesian orbit position coordinates, that is,

$$\boldsymbol{X} = \boldsymbol{\Gamma}(\boldsymbol{\alpha e}) \,, \qquad \text{where} \qquad \boldsymbol{X} \triangleq (\boldsymbol{R}, \dot{\boldsymbol{R}}) \tag{40}$$

The coordinates transformations $\boldsymbol{R}(\boldsymbol{\alpha e})$ and $\dot{\boldsymbol{R}}(\boldsymbol{\alpha e})$ can be written as

$$\boldsymbol{R} = \varrho \, [C(\Omega, i, \omega)] \begin{pmatrix} \cos f \\ \sin f \\ 0 \end{pmatrix} \quad \text{and} \quad \dot{\boldsymbol{R}} = \sqrt{\frac{\mu}{p}} \, [C(\Omega, i, \omega)] \begin{pmatrix} -\sin f \\ e + \cos f \\ 0 \end{pmatrix} \tag{41}$$

where

$$\varrho = \frac{p}{1 + e \cos f} \,, \qquad p = a\big(1 - e^2\big) \,, \qquad \text{and} \qquad f = f(M, e) \tag{42}$$

and

$$[C(\Omega, i, \omega)] = [C_3(-\Omega)][C_1(-i)][C_3(-\omega)] \tag{43}$$

with $[C_i]$ being the single-axis rotation matrix for the i^{th} coordinate axis. While we are expressing position and velocity in terms of true anomaly angle f, differences in mean anomaly M are used to express the relative motion, therefore $f = f(M, e)$. Let $\tilde{}$ denote states of the OEB location

$$\tilde{\boldsymbol{X}} \triangleq \boldsymbol{\Gamma}(\tilde{\boldsymbol{\alpha e}}) \tag{44}$$

The Cartesian formation barycenter (CB) state vector ("true" formation center of mass) is then expressed as

$$\boldsymbol{X}^* \triangleq \frac{1}{M} \sum_{i=1}^{N} m_i \, \boldsymbol{\Gamma}(\tilde{\boldsymbol{\alpha e}} + \delta\boldsymbol{\alpha e}_i) \tag{45}$$

Varying only one of the orbital elements at a time the center of mass error vector becomes

$$\begin{aligned} \Delta\boldsymbol{X} &\triangleq \boldsymbol{X}^* - \tilde{\boldsymbol{X}} \\ &= \frac{1}{M} \sum_{i=1}^{N} m_i \left[\boldsymbol{\Gamma}(\tilde{\boldsymbol{\alpha e}}) + \frac{\partial \boldsymbol{\Gamma}}{\partial \tilde{\alpha e}_i}\bigg|_c \delta\alpha e_i + \frac{1}{2} \frac{\partial^2 \boldsymbol{\Gamma}}{\partial \tilde{\alpha e}_i^2}\bigg|_c \delta\alpha e_i^2 + \mathcal{O}\big(\delta\alpha e_i^3\big) \right] - \boldsymbol{\Gamma}(\tilde{\boldsymbol{\alpha e}}) \\ &= \frac{1}{2M} \frac{\partial^2 \boldsymbol{\Gamma}}{\partial \tilde{\alpha e}_i^2} \sum_{i=1}^{N} m_i \, \delta\alpha e_i^2 + \mathcal{O}\big(\delta\alpha e_i^3\big) \end{aligned} \tag{46}$$

Using similar arguments as were used to derive Eq. (38) first-order terms in Eq. (46) again vanish according to conditions (30). Let us investigate barycenter model deviations behavior further. Using Eq. (46) it is straightforward to show that with $\Delta\boldsymbol{X} = (\Delta\boldsymbol{R}, \Delta\dot{\boldsymbol{R}})$

$$\begin{aligned}\Delta\boldsymbol{R} &= \frac{1}{M}\sum_{i=1}^{N} m_i \left(\sum_{j=2}^{\infty} \frac{1}{j!} \frac{\partial^j \boldsymbol{R}}{\partial \text{œ}_i^j}\bigg|_c (\delta\text{œ}_i)^j \right) \\ &= \frac{1}{M}\sum_{j=2}^{\infty} \frac{1}{j!} \frac{\partial^j \boldsymbol{R}}{\partial \text{œ}^j}\bigg|_c \left(\sum_{i=1}^{N} m_i (\delta\text{œ}_i)^j \right)\end{aligned} \tag{47}$$

and therefore

$$\begin{aligned}\Delta R = \|\Delta\boldsymbol{R}\| &= \frac{1}{M}\frac{1}{2} \left\| \frac{\partial^2 \boldsymbol{R}}{\partial \text{œ}_i^2}\bigg|_c \right\| \left\| \sum_{i=1}^{N} m_i (\delta\text{œ}_i)^2 + \mathcal{R}_{\Delta R}\big(\mathcal{O}(\delta\text{œ}_i)^3\big) \right. \\ &= c_{\Delta R}\, \frac{1}{2M} \sum_{i=1}^{N} m_i (\delta\text{œ}_i)^2 + \mathcal{R}_{\Delta R}\big(\mathcal{O}(\delta\text{œ}_i)^3\big)\end{aligned} \tag{48}$$

where we have introduced the symbol $c_{\Delta R}$ to simplify notation. A similar expression is obtained for $\Delta\dot{R}$ *mutatis mutandis*; the RMS deviation ratio $\gamma(\delta\text{œ}_i)$ then yields

$$\gamma(\delta\text{œ}_i) \triangleq \frac{\Delta\dot{R}}{\Delta R} = \frac{c_{\Delta\dot{R}}}{c_{\Delta R}} \frac{\Big[1 + \tilde{\mathcal{R}}_{\Delta\dot{R}}\big(\mathcal{O}(\delta\text{œ}_i)\big)\Big]}{\Big[1 + \tilde{\mathcal{R}}_{\Delta R}\big(\mathcal{O}(\delta\text{œ}_i)\big)\Big]} = c\,(1 + \mathcal{O}(\delta\text{œ}_i)) \tag{49}$$

Algebraic expressions for RMS deviation approximation constants $c_{\Delta R} = c_{\Delta R}(\boldsymbol{\text{œ}}, \delta\text{œ}_i)$ and $c_{\Delta\dot{R}} = c_{\Delta\dot{R}}(\boldsymbol{\text{œ}}, \delta\text{œ}_i)$ are listed in the Appendix.

As discussed in a previous section, both the Cartesian and the orbital element descriptions provide a meaningful definition for the system barycenter. While traditionally the CB has been used extensively in the literature, the OEB offers distinct advantages for formation control applications. From this point of view it is more adequate to refer to the difference between the two barycenter definitions as *deviations* rather than errors. Consequently, we employ from now on the terminology *center of mass* (or equivalently *barycenter*) *deviation vector* to denote $\Delta\boldsymbol{X}$ and similarly $\Delta\boldsymbol{R}$ and $\Delta\dot{\boldsymbol{R}}$.

Schaub and Alfriend[15] present RMS deviations for a linearized relative motion description using orbital element differences which can be explained analytically using Eq. (46). The RMS deviations show a quadratic behavior in general with the exception of positional deviations due to variations in semi-major axis. In nonlinear mappings between orbit element and inertial Cartesian coordinates in Eq. (40), the satellite semi-major axes a_i appear linearly. Therefore, the position deviation vector yields $\Delta\boldsymbol{R}(\delta\text{œ}_i = \delta a_i) = \boldsymbol{0}$, as expected.

The following numerical simulation illustrates the formation barycenter model deviations. The chief orbital element set is given in Table 1. The individual orbit element differences are varied for each case shown up to a corresponding maximum satellites separation from the formation barycenter of 1000 meters.

Table 1: Chief orbital elements.

Orbital element	a [km]	e	i [°]	Ω [°]	ω [°]	M [°]
Value	6739.6	9.0×10^{-4}	51.7	14.6	-33.0	-19.0

Similarly to results published in Reference 15, Figure 1 illustrates how both RMS position and velocity deviations ΔR and $\Delta\dot{R}$ grow in near-quadratic fashion as the orbit element differences $\delta\text{œ}_i$ are increased. Figure 2 shows $\Delta\dot{R}$ versus ΔR for the same range of orbit element differences. Ten steps are used to sweep the orbit element differences. Note the near-linear behavior plotting $\Delta\dot{R}$ vs. ΔR and predicted by Eq. (49).

With RMS deviation approximation constants readily available (Appendix) we introduce the quantities $\epsilon(\Delta\dot{R})$ and $\epsilon(\Delta R)$ to measure the accuracy of RMS deviation approximations via

$$\epsilon(\Delta R) = \frac{\Delta R - c_{\Delta R}\,\frac{1}{2M}\sum_{i=1}^{N} m_i (\delta\text{œ}_i)^2}{\Delta R} = \frac{\mathcal{R}_{\Delta R}\big(\mathcal{O}(\delta\text{œ}_i)^3\big)}{\Delta R} \qquad \text{and} \qquad \epsilon(\Delta\dot{R}) = \frac{\mathcal{R}_{\Delta\dot{R}}\big(\mathcal{O}(\delta\text{œ}_i)^3\big)}{\Delta\dot{R}} \tag{50}$$

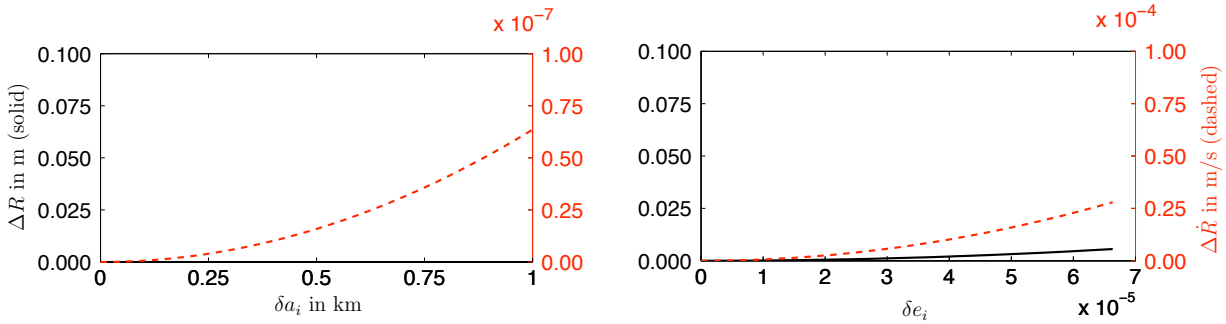

a) C.M. errors for varying δa_i

b) C.M. errors for varying δe_i

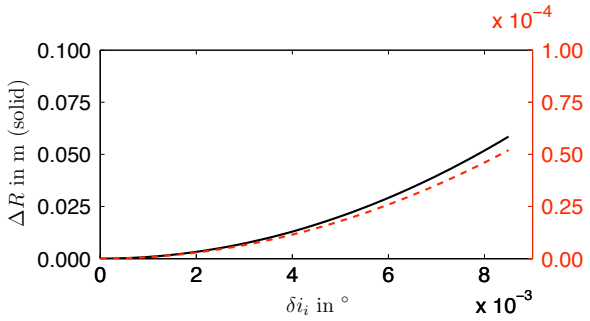

c) C.M. errors for varying δi_i

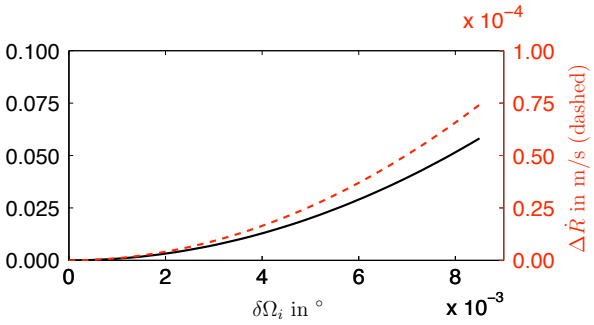

d) C.M. errors for varying $\delta \Omega_i$

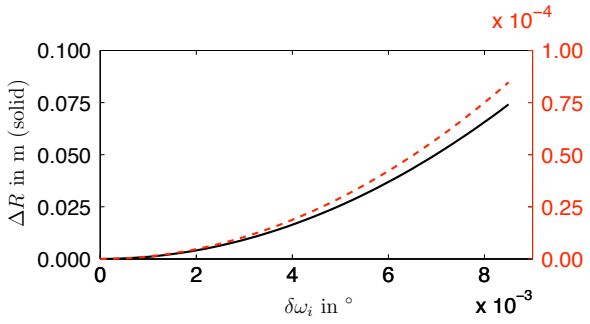

e) C.M. errors for varying $\delta \omega_i$

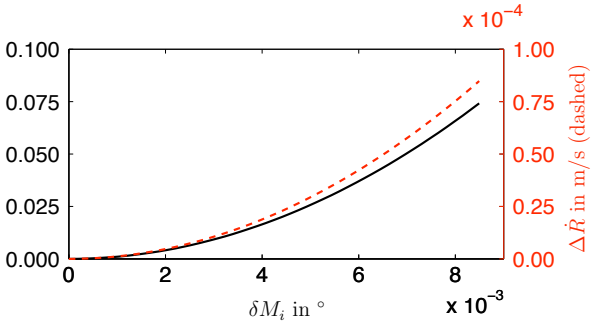

f) C.M. errors for varying δM_i

Figure 1: Center of mass RMS deviations ΔR (solid lines) and $\Delta \dot{R}$ (dashed lines) as a function of orbital element differences $\delta o\!\!\!\!-_i$ for a formation of two spacecraft and a maximal spacecraft-barycenter displacement of 1000 m.

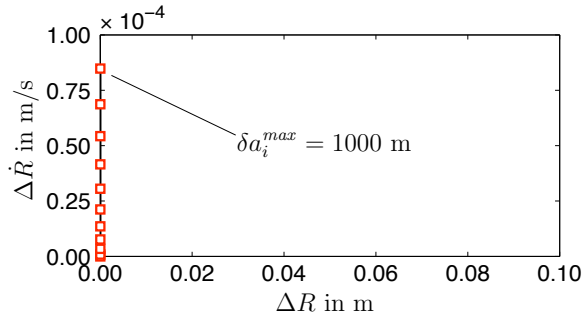

a) C.M. error for varying δa_i

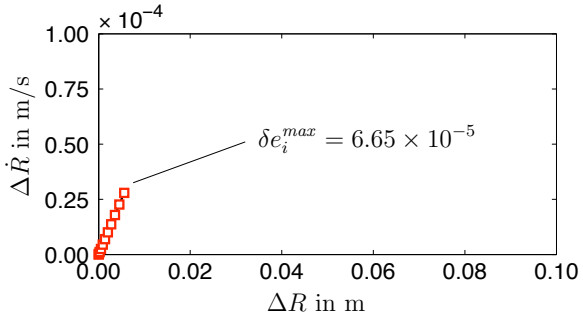

b) C.M. error for varying δe_i

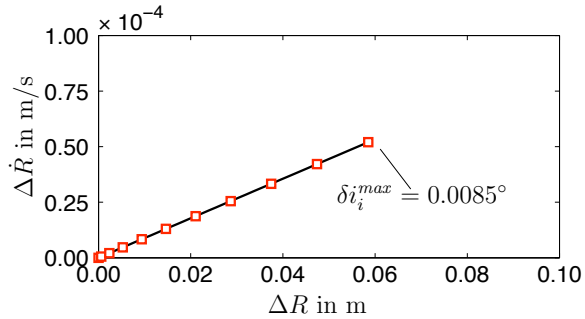

c) C.M. error for varying δi_i

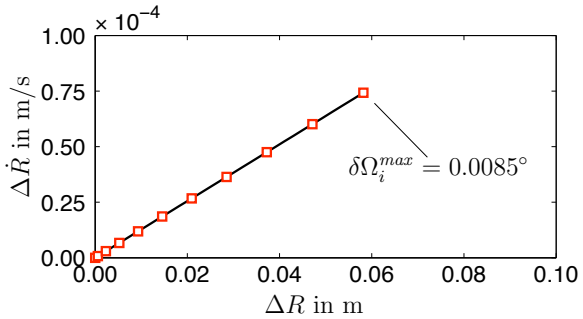

d) C.M. error for varying $\delta\Omega_i$

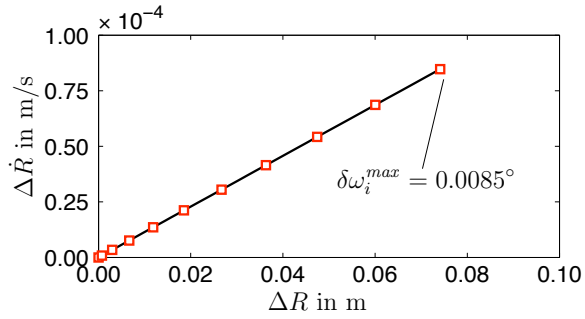

e) C.M. error for varying $\delta\omega_i$

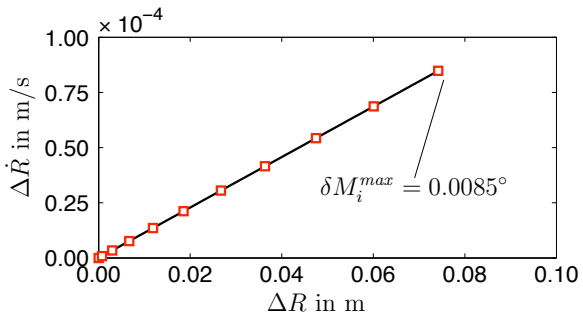

f) C.M. error for varying δM_i

Figure 2: Center of mass RMS deviations $\Delta\dot{R}$ versus ΔR for a formation of two spacecraft and a maximal spacecraft-barycenter displacement of 1000 m. Discrete data points ▫ are plotted using equidistant step sizes $\delta\text{œ}_i$.

For the two-spacecraft formation example Table 2 lists RMS position and velocity deviations and corresponding relative errors $\epsilon(\Delta R)$ and $\epsilon(\Delta\dot{R})$ for a spacecraft-barycenter displacement of 1000 m. The relative error magnitudes justify approximating barycenter deviations using only the first term in the expansion in Eq. (48).

Table 2: Center of mass RMS deviations $\Delta\dot{R}$ and ΔR and relative errors of first-order center of mass RMS deviation approximations $\epsilon(\Delta\dot{R})$ and $\epsilon(\Delta R)$ for a formation of two spacecraft and a spacecraft-barycenter displacement of 1000 m.

$\delta\alpha_i$	$\Delta\dot{R}$ [m/s]	$\epsilon\,(\Delta\dot{R})$ [%]	ΔR [m]	$\epsilon\,(\Delta R)$ [%]
δa_i	6.3545×10^{-5}	3.2974×10^{-7}	0	0
δe_i	2.7945×10^{-5}	5.3899×10^{-3}	5.5828×10^{-3}	2.0733×10^{-2}
δi_i	5.2028×10^{-5}	7.8786×10^{-7}	5.8517×10^{-2}	1.9257×10^{-7}
$\delta\Omega_i$	7.4239×10^{-5}	2.5434×10^{-7}	5.8184×10^{-2}	7.0776×10^{-8}
$\delta\omega_i$	8.4727×10^{-5}	5.2788×10^{-7}	7.4125×10^{-2}	1.5317×10^{-6}
δM_i	8.4791×10^{-5}	1.9782×10^{-7}	7.4181×10^{-2}	3.3985×10^{-8}

VI. Conclusion

First order constraints of Coulomb formations are presented using orbit element differences. The formation chief position is chosen to be the formation center of mass. Because all Coulomb propulsion forces are formation internal forces, the inertial momentum vector of the entire formation is conserved. This constant vector, along with the center of mass definition of the formation chief, impose 6 constraints on the Coulomb formation. Using orbit element differences, first order approximations of the Cartesian barycenter are found. Further, the orbit element barycenter of the formation is introduced. This barycenter definition has advantages if used as a referenced point for formation control laws. The momentum constraint does not yield first order orbit element constraint conditions. Future research will investigate the second order orbit element based momentum constraints. A careful analysis is presented detailing the position and velocity differences between the Cartesian and orbit element barycenter definitions. First order analytical solutions are presented to compute the barycenter differences.

References

[1] King, L. B., Parker, G. G., Deshmukh, S., and Chong, J.-H., "Spacecraft Formation-Flying using Inter-Vehicle Coulomb Forces," Tech. report, NASA/NIAC, January 2002, http://www.niac.usra.edu.

[2] Mullen, E. G., Gussenhoven, M. S., and Hardy, D. A., "SCATHA Survey of High-Voltage Spacecraft Charging in Sunlight," *Journal of the Geophysical Sciences*, Vol. 91, 1986, pp. 1074–1090.

[3] Torkar, K. and et. al., "Active Spacecraft Potential Control for Cluster – Implementation and First Results," *Annales Geophysicae*, Vol. 19, 2001, pp. 1289–1302.

[4] Nicholson, D. R., *Introduction to Plasma Theory*, Krieger, 1992.

[5] Gombosi, T. I., *Physics of the Space Environment*, Cambridge University Press, 1998.

[6] King, L. B., Parker, G. G., Deshmukh, S., and Chong, J.-H., "Study of Interspacecraft Coulomb Forces and Implications for Formation Flying," *AIAA Journal of Propulsion and Power*, Vol. 19, No. 3, May–June 2003, pp. 497–505.

[7] Schaub, H., Parker, G. G., and King, L. B., "Challenges and Prospect of Coulomb Formations," *AAS John L. Junkins Astrodynamics Symposium*, College Station, TX, May 23-24 2003, Paper No. AAS-03-278.

[8] Schaub, H., "Stabilization of Satellite Motion Relative to a Coulomb Spacecraft Formation," *AAS Space Flight Mechanics Meeting*, Maui, Hawaii, Feb. 8–12 2004.

[9] Joe, H., Schaub, H., and Parker, G. G., "Formation Dynamics of Coulomb Satellites," *6th International Conference on Dynamics and Control of Systems and Structures in Space*, Riomaggiore, Cinque Terre, Italy, July 2004.

[10] Schaub, H. and Junkins, J. L., *Analytical Mechanics of Space Systems*, AIAA Education Series, Reston, VA, October 2003.

[11] Hill, G. W., "Researches in the Lunar Theory," *American Journal of Mathematics*, Vol. 1, No. 1, 1878, pp. 5–26.

[12] Clohessy, W. H. and Wiltshire, R. S., "Terminal Guidance System for Satellite Rendezvous," *Journal of the Aerospace Sciences*, Vol. 27, No. 9, Sept. 1960, pp. 653–658.

[13] Schaub, H., "Spacecraft Relative Orbit Geometry Description Through Orbit Element Differences," *14th U.S. National Congress of Theoretical and Applied Mechanics*, Blacksburg, VA, June 2002.

[14] Schaub, H., "Relative Orbit Geometry Through Classical Orbit Element Differences," *Journal of Guidance, Control and Dynamics*, 2004, accepted for publication.

[15] Schaub, H. and Alfriend, K. T., "Hybrid Cartesian and Orbit Element Feedback Law for Formation Flying Spacecraft," *Journal of Guidance, Control and Dynamics*, Vol. 25, No. 2, March–April 2002, pp. 387–393.

VII. Appendix

In starting to analyze mappings (41), we notice that the coordinate transformations can be written as products $[C(\Omega, i, \omega)]\,\boldsymbol{\xi}(a, e, f(M, e))$. Therefore, when evaluating derivatives with respect to a particular orbital element one needs to focus only on either the rotation matrix or the respective vector $\boldsymbol{\xi}$. We further note that for our analysis the true anomaly is treated as a dependent variable, depending on independent variables M and e.

Calculations of deviation constants $c_{\Delta\dot{R}}$ and $c_{\Delta R}$ for semimajor axis variations are straightforward. Deviation constant computations for variations in orbit orientation parameters $\{\Omega, i, \omega\}$ are facilitated by hand by using Singular Value Decompositions (SVD) for the particular rotation matrix. Note that

$$\frac{d^2}{d\alpha^2}[C_j(\alpha)] = [U(\alpha)]_j[S]_j[V]_j\ , \qquad i = 1, 2, 3 \tag{51}$$

where $|\det([U]_j)| = 1$, $[S]_j$ projects vectors onto the 1–2 plane and $[V]_j$ essentially simply reorders vector components. For the inclination angle, for example, the problem of calculating $(d^2/di^2)\,[C(\Omega, i, \omega)]$ can therefore be replaced by the problem of computing $[S]_1[V]_1[C_3(-\omega)]$. A similar analysis can be performed to yield deviation constants for the ascending node angle and the argument of periapses.

Deviation constants for mean anomaly variations and eccentricity variations are more complex since mappings (41) are expressed using true anomaly and $f = f(M, e)$ as pointed out before. For eccentricity variations $c_{\Delta\dot{R}}$ and $c_{\Delta R}$ are therefore calculated (using operator notation) $[d/de]^2\,(\cdot) \doteq \left[\partial/\partial e + (\partial f/\partial e)(\partial/\partial f)\right]^2(\cdot)$. Deviation constants for mean anomaly variations are obtained in a similar fashion.

Table 3: First-order center of mass RMS deviation constants $c_{\Delta\dot{R}}$ and $c_{\Delta R}$.

$$\left\| \left. \frac{\partial^2 \dot{\boldsymbol{R}}}{\partial a_i^2} \right|_c \right\| = \sqrt{\frac{\mu}{p}} \frac{3}{4a^2} \sqrt{1 + 2e\cos f + e^2} \tag{52}$$

$$\left\| \left. \frac{\partial^2 \dot{\boldsymbol{R}}}{\partial e_i^2} \right|_c \right\| = \sqrt{\frac{\mu}{p}} \frac{1}{16(1-e^2)^2} \left\{ \Big[-20\,e + 2\big(-10 + 9\,e^2\big)\cos f + 48\,e\cos(2f) + \big(36 + 11\,e^2\big)\cos(3f) + 20\,e\cos(4f) + 3\,e^2\cos(5f) \Big]^2 + 4\Big[12 + 29\,e^2 + 76\,e\cos f + 4\big(9 + 4\,e^2\big)\cos(2f) + 20\,e\cos(3f) + 3\,e^2\cos(4f) \Big]^2 \sin^2 f \right\}^{1/2} \tag{53}$$

$$\left\| \left. \frac{\partial^2 \dot{\boldsymbol{R}}}{\partial i_i^2} \right|_c \right\| = \sqrt{\frac{\mu}{p}} \left| \cos(\omega + f) + e\cos\omega \right| \tag{54}$$

$$\left\| \left. \frac{\partial^2 \dot{\boldsymbol{R}}}{\partial \Omega_i^2} \right|_c \right\| = \sqrt{\frac{\mu}{p}} \sqrt{1 + 2e\cos f + e^2 - \sin^2 i \left[e\cos\omega + \cos(\omega + f) \right]^2} \tag{55}$$

$$\left\| \left. \frac{\partial^2 \dot{\boldsymbol{R}}}{\partial \omega_i^2} \right|_c \right\| = \sqrt{\frac{\mu}{p}} \sqrt{1 + 2e\cos f + e^2} \tag{56}$$

$$\left\| \left. \frac{\partial^2 \dot{\boldsymbol{R}}}{\partial M_i^2} \right|_c \right\| = \sqrt{\frac{\mu}{p}} \frac{(1 + e\cos f)^3}{(1-e^2)^3} \sqrt{\frac{2 + 4e\cos f + 5e^2 - 3e^2\cos(2f)}{2}} \tag{57}$$

$$\left\| \left. \frac{\partial^2 \boldsymbol{R}}{\partial a_i^2} \right|_c \right\| = 0 \tag{58}$$

$$\left\| \left. \frac{\partial^2 \boldsymbol{R}}{\partial e_i^2} \right|_c \right\| = \frac{p}{(1 + e\cos f)} \frac{|\sin f|}{\sqrt{8}(1-e^2)} \sqrt{20 - 12\cos(2f) + 8e\left[5\cos f - \cos(3f)\right] + e^2[33 - \cos(4f)]} \tag{59}$$

$$\left\| \left. \frac{\partial^2 \boldsymbol{R}}{\partial i_i^2} \right|_c \right\| = \frac{p}{1 + e\cos f} \left| \sin(\omega + f) \right| \tag{60}$$

$$\left\| \left. \frac{\partial^2 \boldsymbol{R}}{\partial \Omega_i^2} \right|_c \right\| = \frac{p}{1 + e\cos f} \sqrt{1 - \sin^2 i \sin^2(\omega + f)} \tag{61}$$

$$\left\| \left. \frac{\partial^2 \boldsymbol{R}}{\partial \omega_i^2} \right|_c \right\| = \frac{p}{1 + e\cos f} \tag{62}$$

$$\left\| \left. \frac{\partial^2 \boldsymbol{R}}{\partial M_i^2} \right|_c \right\| = \frac{a\,(1 + e\cos f)^2}{(1-e^2)^2} \tag{63}$$